Journal of Power Sources 257 (2014) 344–355

Contents lists available at ScienceDirect

Journal of Power Sources

journal homepage: www.elsevier.com/locate/jpowsour

A theoretical and computational study of lithium-ion battery thermal management for electric vehicles using heat pipes

Angelo Greco [a], Dongpu Cao [b], Xi Jiang [a,*], Hong Yang [c]

[a] Department of Engineering, Lancaster University, Lancaster LA1 4YR, UK
[b] Department of Automotive Engineering, Cranfield University, Bedford MK43 0AL, UK
[c] McMaster University, Hamilton, ON L8S 4L8, Canada

HIGHLIGHTS

- Battery thermal management using heat pipes is considered.
- The heat pipe set is arranged in a sandwiched configuration to enhance the cooling.
- A one-dimensional (1D) model using the thermal circuit method is proposed.
- The simplified 1D model is in good agreement with the analytical solution.
- The 1D model is also in agreement with the corresponding 3D CFD results.

ARTICLE INFO

Article history:
Received 9 December 2013
Received in revised form
30 January 2014
Accepted 1 February 2014
Available online 11 February 2014

Keywords:
Battery thermal management
Heat pipe
Li-ion battery
Passive cooling management
Thermal network model

ABSTRACT

A simplified one-dimensional transient computational model of a prismatic lithium-ion battery cell is developed using thermal circuit approach in conjunction with the thermal model of the heat pipe. The proposed model is compared to an analytical solution based on variable separation as well as three-dimensional (3D) computational fluid dynamics (CFD) simulations. The three approaches, i.e. the 1D computational model, analytical solution, and 3D CFD simulations, yielded nearly identical results for the thermal behaviours. Therefore the 1D model is considered to be sufficient to predict the temperature distribution of lithium-ion battery thermal management using heat pipes. Moreover, a maximum temperature of 27.6 °C was predicted for the design of the heat pipe setup in a distributed configuration, while a maximum temperature of 51.5 °C was predicted when forced convection was applied to the same configuration. The higher surface contact of the heat pipes allows a better cooling management compared to forced convection cooling. Accordingly, heat pipes can be used to achieve effective thermal management of a battery pack with confined surface areas.

1. Introduction

Electrical vehicles can be used to reduce the emissions from the traditional internal combustion engine powered vehicles. A wider spread usage of electrical vehicles depends on the development of rechargeable batteries. Lithium-ion (Li-ion) battery has been dominantly utilised for electric vehicles, due to its excellent performance characteristics, such as high energy density, long life-time and low self-discharge. However, its narrow desirable operating temperature range imposes a significant challenge on the thermal management of Li-ion batteries. Thermal management of Li-ion batteries is crucial to safety issues like thermal runaway or overheating during operation. These issues can strongly affect the battery performances and lifespan. In addition, more research needs to be done for transport applications of Li-ion batteries where high electric power is used in a relatively short time period.

It has been shown that temperature affects the longevity, efficiency, and safety of the battery. Thermal runaway, electrolyte fire, and in certain cases explosions [1] can occur when the temperature in the battery is too high. Therefore, an efficient battery thermal management system (BTMS) is required in order to maintain the battery temperature between 20 °C and 40 °C [2]. Moreover, to avoid any short circuit leading potentially to destroy the battery, an even temperature distribution must be achieved in the battery module and pack. For achieving a uniform temperature

* Corresponding author. Tel.: +44 1524 592439.
E-mail addresses: x.jiang@lancaster.ac.uk, qmwxjiang@hotmail.com (X. Jiang).

http://dx.doi.org/10.1016/j.jpowsour.2014.02.004
0378-7753/

Nomenclature

a	height of the groove channel [m]
b	width of the groove channel [m]
$[C]$	matrix of the thermal capacitance [J K^{-1}]
e_b	thickness of the battery cell [m]
F	Faraday constant [C mol^{-1}]
$[G]$	matrix of the conductance [W K^{-1}]
h_{conv}	heat transfer coefficient for natural convection [W m^{-2} K^{-1}]
h_{fg}	specific enthalpy [J kg^{-1}]
i	discharge current per unit volume [A m^{-3}]
k	thermal conductivity [W m^{-1} K^{-1}]
K	permeability of the capillary structure [m^2]
k_{wall}	thermal conductivity of the heat pipe material envelop [W m^{-1} K^{-1}]
L_{adia}	length of the adiabatic section [m]
l_b	width of the battery cell [m]
L_b	length of the battery cell [m]
L_c	length of the condenser section [m]
L_{ev}	length of the evaporator section [m]
L_{total}	length of the heat pipe [m]
M	working fluid merit number [m^2]
n	number of electron exchange during the discharge
N_C	capillary number [W m^{-2}]
N_{GS}	number of groove section in one heat pipe
N_{HP}	number of heat pipe in the set
$[P]$	matrix of internal power [W]
q	internal heat generation in the battery [W m^{-3}]
Q_{max}	capillary limit [W]
R	radius [m]
R_i	internal equivalent resistance per unit volume [Ω m^3]
S	entropy [J mol^{-1} K^{-1}]
S_b	surface of the battery cell at $x = e_b$ [m^2]
S_l	liquid section of the heat pipe [m^2]
$[T]$	matrix of the temperature [°C]

Greek letters

Δ	variation
Θ	thermo-physical property group [m^2]
μ	viscosity [kg m^{-1} s^{-1}]
ρ	density [kg m^{-3}]
Φ	geometric dimensions group [m^2]
σ	surface tension [N m^{-1}]
Ψ	dimensionless number defined in Eq. (16) [19]

Subscripts

adia	adiabatic
amb	ambient
c	condenser
ev	evaporator
GS	groove section
HP	heat pipe
v	vapour
x, y, z	coordinates

distribution, the temperature difference from cell to cell and module to module should be normally within 5 °C.

The thermal behaviour of the battery is strongly coupled to the electrochemical process. To simplify the analysis, the heat generated by exothermic chemical reaction during discharge can be represented by a global term linked to the major electrochemical characteristics. Gao et al. [3] modelled the transient behaviour of a commercial Li-Ion battery using an equivalent electric circuit. Based on their work, Chen et al. [4] simplified the mathematical solution. However, these simplified models were not sufficiently developed to describe the temperature distribution in a battery cell to aid the design of the thermal management system.

Different two- and three-dimensional (2D and 3D) numerical models of temperature prediction were developed in the past. Inui et al. [5] developed 2D and 3D codes for cylindrical and prismatic shaped batteries respectively, to predict the transient distribution of temperature during discharge. Karimi and Li [6] extended the study by Inui et al. to a 2D numerical simulation of an entire pack of prismatic battery cooled by natural and forced convection. They also demonstrated that a distributed configuration of the cooling system was the best solution to maintain an equal temperature distribution in the battery pack (stack of prismatic battery cell).

Three-dimensional numerical simulations using global thermo-physical properties to represent the physical properties of the battery multi-layer structure were carried out [7,8]. The battery was cooled by active air cooling and the results showed a good agreement between simulations and measurements. Taheri et al. [9] developed a 3D analytical model to predict the transient thermal behaviour of a Li-ion battery cell cooled by convection. The modelling was based on integral-transform technique and used an internal heat generation term. The derived analytical solution was efficient to compute the different values of convective heat coefficient applied at different positions of the battery cell. A surface averaged Biot number was proposed to simplify the solutions in 1D or 2D depending on the value of thermo-physical properties of the battery and the heat transfer coefficient applied on the battery's surfaces.

Researches have also been performed on effective thermal control of the battery pack. Pesaran [10] showed that for heat exchanger design, a parallel cooling flow was effective in order to achieve an even temperature distribution in the battery pack. Chacko [11] used a liquid cooling plate composed of a serpentine channel, but this configuration was not developed to achieve an even temperature distribution. Mahamud and Park [12] performed a numerical analysis of cylindrical cells cooled by reciprocating air flow. Their results showed a 4 °C decrease in the temperature difference in the battery pack.

Active air or liquid flow convection as a cooling solution implies a bulky flow management system and additional costs due to the maintenance and the weight. Therefore, as an alternative method, passive cooling management (PCM) is investigated as a BTMS solution, especially for confined spaces where intensive heat transfer is required. For example, phase change materials [13,14] are very simple to use, but their low conductivity limits their applications. A possible solution for further improvements is to add a high conductive matrix in the structure of the phase change materials to enhance the thermal conductivity.

Wu et al. [15] showed experimentally the importance of a good surface contact between the heat pipe and the battery in achieving effective cooling. Rao et al. [16] performed experimental studies of a prismatic shape battery cooled by heat pipes. Their results showed a maximum battery cell temperature under 50 °C for a heat generation rate lower than 50 W and a temperature variation within 5 °C for a heat generation rate not exceeding 30 W. This work can be completed by analysing the impact of heat pipe on the temperature distribution of the battery cell or pack. Besides, further

studies need to be done to choose or design the right heat pipes according to the maximum range of temperature reached by the battery cell. In general, there is still a lack of understanding on the effectiveness of heat pipes used as a PCM system solution.

This work was motivated by the need to develop reliable and possibly simple methods to analyse heat pipes used as a PCM solution, in order to guide the BTMS design. A study of a prismatic battery cell, cooled by heat pipes during constant-current discharge rate, is performed using different computational/analytical methods. The heat pipe used for the simulations was designed according to the maximum heat generated by the battery cell. The transient thermal behaviour of the heat pipe was modelled by a thermal network method [17–20]. The battery cell used in this study was the ePLB C020 battery (capacity of 20 Ah), fabricated by EiG Corporation, Korea. All simulations were performed using geometrical and electrochemical characteristics from the literature [9]. The other objective is to show that with the right design, heat pipes are able to remove more heat much quicker than normal active cooling. For conservatism in the design, the simulation was performed with the maximum discharge rate of 5 C, corresponding to a discharge current of 100 A.

This paper presents results from a study numerically and analytically investigating the PCM of a Li-ion battery cell using heat pipes. Different configurations were studied and compared to forced convection during a constant current discharge process. The transient computational model based on the thermal circuit method is 1D and consistent with the analytical solution, while the numerical simulation was performed in 3D. The paper presents the cooling system and heat pipe design first, followed by descriptions of the model development including the heat pipe and thermal models, and descriptions of the three different approaches. Results and discussions are then presented. Finally, some conclusions are drawn.

2. Design of the battery cooling system

A generic battery cooling system design is shown in Fig. 1, where the heat pipes are integrated within a copper structure that allows a desirable conductive heat transfer between the battery and the heat pipe set. To cover the entire surface of the battery cell and enhance the heat transfer, eighteen heat pipes with a 10 mm diameter and a 0.8 mm gap are considered in this design. For a battery pack with a number of cells, the battery cooling system can be designed using a layout with alternate battery cell and heat pipe set. For the understanding of the effectiveness of the system, it is crucial to understand the fundamental heat transfer characteristics of a single battery cell in conjunction with the heat pipe set.

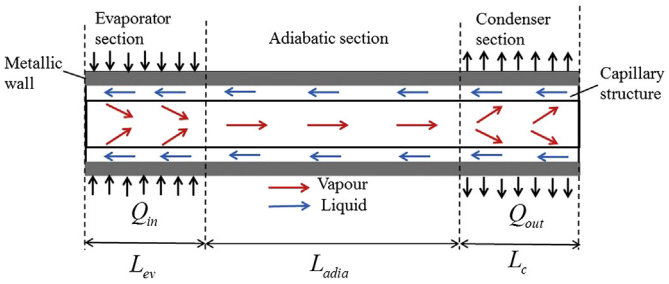

Fig. 2. Schematic of the heat transfer working principle of a heat pipe.

Fig. 2 depicts the heat transfer principle of a heat pipe, where the heat pipe is a tube filled by a working fluid in a saturated state. When the evaporator section is heated up, vapour is generated and carries the heat to the condenser section where the heat pipe is usually cooled down by convection. Then, the liquid in the condenser section is brought back to the evaporator by the capillary forces, as seen in Fig. 2. The capillary forces can be increased by an addition of a wick or groove structure, which will be discussed later in Fig. 3. Therefore, the process works continuously as long as the evaporator is heated and the condenser is cooled.

However, there are a number of limits on the heat pipe heat transfer capacity (or efficiency), due to the thermo-physical properties of the working fluid, the geometry of the heat pipe as well as the friction in the fluid channels. In this analysis, only the capillary limit is considered, which refers to the maximum heat transferrable by the heat pipe without stopping the return of the fluid from the condenser to the evaporator. The analytical formulations for this limit take into account the capillary forces and the friction in the channels (liquid and vapour). The influence of the gravity was not included in the analysis because the heat pipe can be arranged in a horizontal position. However, it is worth noting that the gravity helps to improve the capillary limit when the cooling system is arranged in a thermo-siphon configuration [17].

The choice of working fluid has an influence on the heat transfer capacity of the heat pipe. Working fluid with a high wettability and chemical stability for the pipe material is desirable. In addition, the operating temperature of the battery cell needs to be kept within the saturated state temperature interval of the working fluid. The

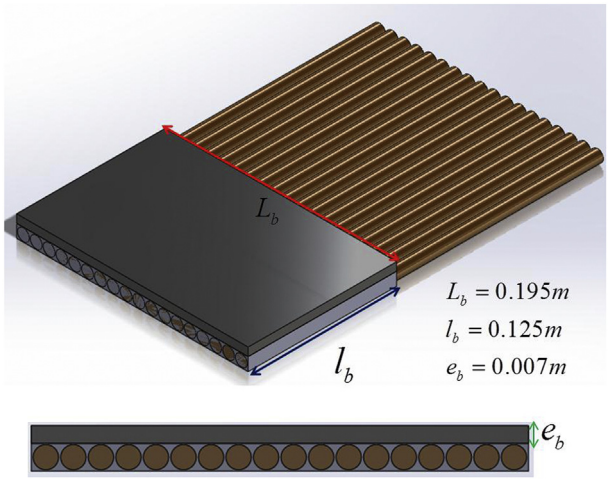

Fig. 1. The design of the generic battery cooling system using heat pipes.

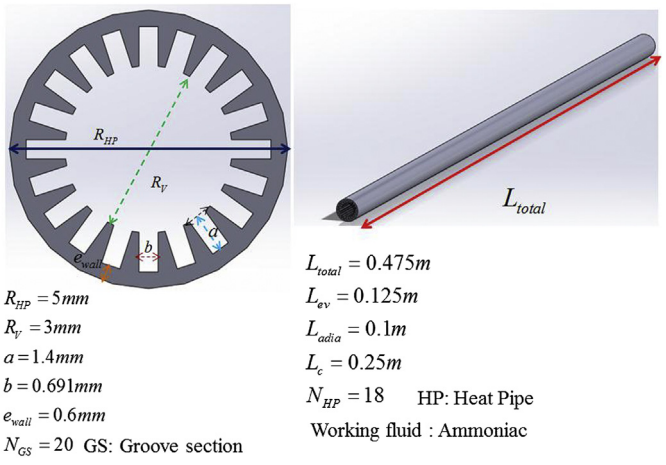

Fig. 3. The design and geometrical properties of the heat pipe with a groove structure.

pressure drop in the vapour channel is much lower compared to the pressure drop in the liquid channel. The pressure drop in the vapour channel is thus assumed to be negligible to simplify the calculations. Based on the above considerations and assumptions, the capillary limit is calculated as follows [17,18]:

$$Q_{max} = N_C{}^*M \quad \text{with } N_C = \frac{2S_l K}{bL_{eff}} \text{ and } M = \frac{\sigma\rho_l h_{fg}}{\mu_l} \tag{1}$$

where the capillary number N_C can be used to choose the groove section (as shown in Fig. 3), and is also related to the dimensions of the heat pipe. The working fluid merit number M can be used to select the working fluid. The larger the merit number is, the higher the capillary limit will be.

Fig. 3 shows the design of a single heat pipe with a groove structure. In this study, the maximum transferrable heat power by a single heat pipe is chosen to be 400 W, as an example. The heat pipe is oversized to reflect the design conservatism in terms of the 41 W maximum power generated by the battery. This design choice is made in order to assure an effective working process during discharge, but also for the purpose of future experimental study. The geometrical parameters of the heat pipe are determined accordingly and presented in Fig. 3. Heat transfer analysis of a single heat pipe is complex, since different phenomena need to be considered, such as thermal conduction, phase change, and fluid dynamics. CFD simulations and analyses have been broadly used including those using commercial software packages. However, the CFD approach is often very costly in terms of computing resources needed and requires validations especially for changed conditions. Due to these reasons, simplified models are often used in practical applications.

3. Problem description and modelling simplification

A 3D numerical simulation of a battery pack cooled by heat pipes is complex and time consuming. In the case of simulating one pipe, it will also necessitate high computing resources in order to describe the mass and heat transfer, during the transient discharge of the battery. In light of this, another computationally efficient approach is adopted. The thermal behaviour of the battery is modelled by a thermal network using the thermal circuit method. Additionally, for the temperature prediction of a detailed battery cell (multi-layer structure), considering the electro-chemical reactions is also too complex to execute. Therefore, models are proposed to simulate the heat generation due to the electro-chemical reaction of the battery and to describe the thermal properties of the multi-layer structure of the battery cell.

3.1. Model formulation of the heat pipe

Zuo and Faghri [19] developed a thermal network model of heat pipe that showed a good agreement with the experimental data. In this study, a further simplified thermal network is proposed, as shown in Fig. 4. In this model, the thermal resistances R_{th3} and R_{th5} are due to the phase change, while the thermal resistance R_{th4} is due to the flow of vapour. Because of the high thermal conductance ($G_{th} \approx 10^5$) of these heat transfers, the thermal resistance R_{th3}, R_{th4} and R_{th5}, can be neglected ($G_{th} = 1/R_{th}$).

A macroscopic approach based on parallel or series heat transfer is used to calculate the thermal resistances of the network. The porous media in the heat pipe (wick or groove section) should be taken into account. This modelling method is based on the heat pipe geometry and the choice of the porous media. G_{th1} and G_{th7}, representing the thermal conductance per surface, are calculated from k_{wall}/e_{wall}, where k_{wall} is the thermal conductivity of the heat

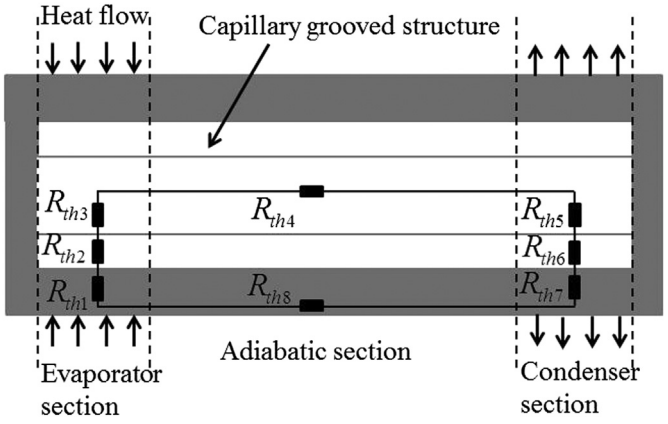

Fig. 4. Thermal network of a heat pipe.

pipe material envelop and e_{wall} is the thickness of the wall. For the evaporating area (G_{th2}) containing the groove section and the liquid (seen in Fig. 5(a)), the Chi model [17] is used to determine an equivalent thermal conductivity:

$$k_{ev} = \frac{(k_l k_s AE) + Wk_l(0.185Ek_s + Ak_l)}{(W+E)(0.185Ek_s + Ak_l)} \text{ and } G_{th2} = \frac{k_{ev}}{A} \tag{2}$$

The Chi model is obtained by considering two paths for the heat flux [17]. The first one is a series conduction between the groove structure and a liquid film with thickness of 0.185E. The second path is a parallel conduction pattern between the series pattern presented and a liquid film with a thickness of A. The thermal conductivity of the condensing area (Fig. 5(b)) is calculated using a series pattern $G_{th6} = (A(W+E)/(Wk_l + Ek_s))^{-1}$. However in this formula, the liquid film is not taken into account. Romestant [17] showed that this film can have a strong impact on the thermal conductance, and recommended to divide G_{th6} by 100 to calibrate the impact of the film, based on the experimental results. Finally, G_{th8} is neglected due to the small thickness of the envelop and the length of the heat pipe.

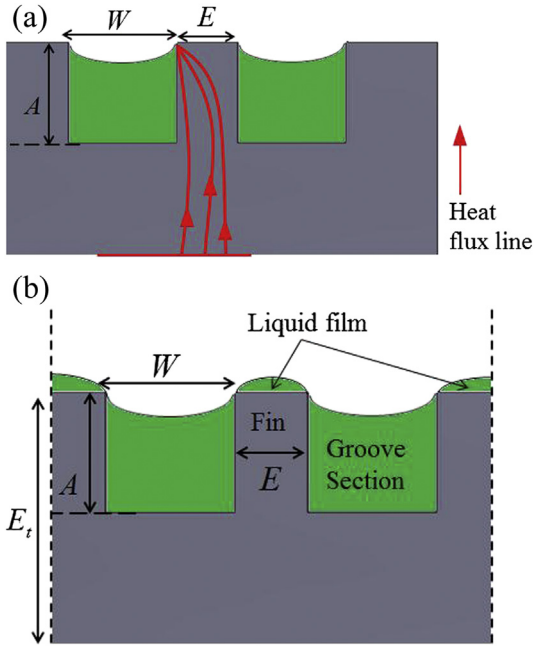

Fig. 5. Groove structure at: (a) the evaporator; and (b) the condenser.

Based on the above modelling assumptions and simplifications, the final thermal network model obtained for the heat pipe is presented in Fig. 6. The thermal network of the heat pipe is composed of 4 nodes. Each section has 2 nodes: one node for the vapour and the other for the wall or envelop of the heat pipe.

3.2. Thermal model formulation of the battery

Different models of heat generation exist in the literature, for representing the internal source term of the battery during discharging. The heat generation rate per volume in a battery cell is calculated, by adopting the following model [5]:

$$q = R_i i^2 - T\Delta Si/(nF) \quad (3)$$

In the above equation, the first term, $R_i i^2$, represents the heat due to the internal equivalent resistance, and the second term, $T\Delta Si/(nF)$, represents the reversible heat caused by the entropy change of electrochemical reactions.

The battery used in this study is the same as that in the literature [9], where only geometrical and nominal thermo-physical characteristics of the battery are available and summarised in Table 1. The source term is assumed to be a constant value during the entire discharging process. The value of the source term is taken as the maximum power generated by the battery during the highest supportable constant-current discharge rate (5 C discharge rate corresponding to 100 A for a capacity of 20 Ah) [9]. In this study, the heat generation rate per volume q is assumed to be 240 kW m^{-3}.

For modelling the battery properties, global thermo-physical properties can be used to represent the physical properties of the battery multi-layer structure. This simplification approach has been validated using the experimental data and used in CFD simulation analyses [7,8]. Moreover, Taheri et al. [9] used this approach to represent the thermo-physical properties of the battery in their 3D analytical model. Based on the geometrical characteristics and thermo-physical properties of the battery multi-layer structure given in Table 1, the global properties are calculated as follows [7–9]:

$$k_x = \frac{\sum_{j=1}^{N} l_j}{\sum_{j=1}^{N} (l_j/k_j)};\ k_y = k_z = \frac{\sum_{j=1}^{N} l_j k_j}{\sum_{j=1}^{N} l_j};\ \rho c_p = \frac{\sum_{j=1}^{N} \rho_j c_{p_j} v_j}{v} \quad (4)$$

The following results are then obtained: $k_x = 0.97\ \mathrm{W/(m\,K)^{-1}}$; $k_y = k_z = 26.57\ \mathrm{W/(m\,K)^{-1}}$; $\rho c_p = 2767.45\ \mathrm{KJ/(m^3\,K)^{-1}}$.

4. Research methods: analytical solution, 1D model and 3D numerical simulation

In this study, the 1D approach is composed of a 1D model (analytical or computational) of the battery, connected to the thermal network model of the heat pipe. Such simplified 1D approach is expected to sufficiently predict the transient thermal behaviour of the battery cooled in different configurations including forced convection and heat pipe sets. The 1D analytical model of the battery is used as a baseline reference in this study, for which the solution developed takes into account the transient behaviour of the cooling process applied on the battery surfaces. A 3D numerical model of the battery cell is simulated using a commercial CFD code, in order to verify the reliability of the 1D approach.

Table 1
Mechanical characteristics and thermo-physical properties of the battery ([9]).

Material layer	Thickness [m]	Number of layers	Density [kg m^{-3}]	Heat capacity [J kg^{-1} K^{-1}]
Aluminium foil	2.10E-05	17	2702	903
Copper foil	1.20E-05	18	8933	385
Separator sheet	2.50E-05	36	1017	1978
Positive electrode	7.00E-05	34	2895	1270
Negative electrode	7.90E-05	36	1555	1437

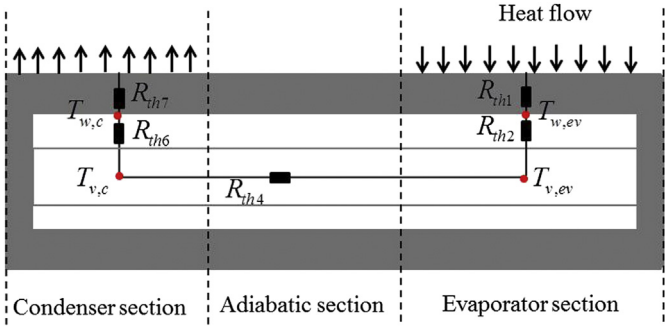

Fig. 6. The simplified thermal network of the heat pipe.

4.1. One-dimensional analytical model

The transient energy equation for temperature of the battery cell cooling by the heat pipes is solved using the separation of variable method [21]. This method necessitates homogeneous and linear boundary conditions for the equation to be applied. Besides, the time dependence of certain boundary conditions of the heat pipe has added further complexities to apply the method. Therefore, simplifications are needed in order to reduce the complexity of the solution. The battery studied belongs to a battery type where an orthotropic conductivity is observed and the thickness direction (x direction in Fig. 7) has a very low conductivity compared to the other directions (y and z directions in Fig. 7). According to this battery's characteristic, the largest gradient of temperature will be in the x direction. Additionally, the heat pipe cooling is also located in the same direction (x direction in Fig. 7). Consequently, it is reasonable to expect that all the important physics of the heat transfer will be represented in this particular direction. This assumption has helped to apply the separation of variable method despite the difficulties enumerated before and has led to a 1D analytical solution, which is very easy to use. However, the intensity of the cooling on the other surfaces of the battery located in the y and z directions can have an impact on the model proposed, and a comparison with a 3D resolution by CFD is performed (described in Sub-section 5.1) in order to verify the assumption made. Finally, the energy equation for temperature in 1D is:

$$C\frac{\partial T}{\partial t} - k_x\frac{\partial^2 T}{\partial x^2} = R_i i^2 \text{ and } \begin{cases} q = R_i i^2 \\ C = \rho c_p \end{cases} \quad (5)$$

The domain of study is shown in Fig. 7:

The 1D thermal equation of the battery cooling is finally solved using the separation of variables method. However, the solution found needs the vapour temperature function of the heat pipe. This vapour temperature function can be obtained experimentally. At

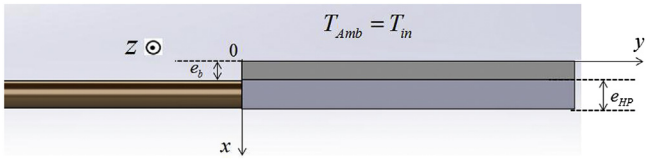

Fig. 7. The 1D domain of study.

$x = e_b$, the boundary condition due to the heat exchange between the battery cell and the heat pipe is represented by:

$$-k_x S\frac{\partial T}{\partial x}(x = e_b, t) = \frac{k_{ev}A_{ev}}{\lambda_{ev}}(T - T_v)(x = e_b, t) \quad (6)$$

This condition is transformed to the following formulation, using a variable change necessary for the separation of variables:

$$\left(k_x S\frac{\partial(T - T_{in})}{\partial x} + \frac{k_{ev}A_{ev}}{\lambda_{ev}}(T - T_{in})\right)(x = e_b, t) = f(t) \quad (7)$$

where $f(t)$ is a function taking into account the conductivity of the evaporator and the vapour temperature in time. Therefore, the complete temperature of the battery can be obtained, by knowing the temperature of the vapour experimentally. Moreover, $f(t)$ can be any function corresponding to different cooling solutions. The only condition needs to satisfy is $f(t = 0) = 0$ in order to apply the separation of variables.

In this study, two analytical solutions are proposed for two different types of boundary conditions. The first type (Case 1) is derived in view of a theoretical case for testing the function and different hypotheses. In this case, one side of the battery has a fixed temperature and the other side is cooled by the heat pipe. The second type (Case 2) is formulated for a battery cell sandwiched between two sets of heat pipes.

- Case 1:

The boundary conditions are presented as follows (Fig. 7):

$$\begin{aligned} &T(x,0) - T_{in} = 0 \\ &T(0,t) - T_{in} = 0 \qquad\qquad f(t) = F(T_v(t) - T_{in}) \\ &\left(\tfrac{\partial(T-T_{in})}{\partial x} + \tfrac{k_{ev}A_{ev}}{\lambda_{ev}k_xS_b}(T - T_{in})\right)(x = e_b, t) = f(t) \quad \text{with} \quad F = \tfrac{k_{ev}A_{ev}}{\lambda_{ev}k_xS_b} \\ &f(t = 0) = 0 \end{aligned} \quad (8)$$

And the solution can be derived as:

$$T_i(x,t) - T_{in} = \sum_{n=0}^{\infty}(H_0(t) - H_0(0)\exp(-\gamma_n t))\sin(\beta_n x) + \frac{x(x - e_b)}{e_b}f(t) \quad (9a)$$

$$\Omega_n H_0(t) = \left(\frac{2[1 - \cos(\beta_n e_b)]}{e_b\beta_n^3} - \frac{\sin(\beta_n e_b)}{\beta_n^2}\right)f(t) + \frac{[1 - \cos(\beta_n e_b)]R_i i^2}{k_x\beta_n^3} + \left(\frac{k_x \sin(\beta_n e_b)}{C}\right) \times \left[\int_0^t f(t)\exp(\gamma_n t)dt\right]\exp(-\gamma_n t) \quad (9b)$$

$$\Omega_n = \frac{\beta_n e_b - \cos(\beta_n e_b)\sin(\beta_n e_b)}{2\beta_n} \quad (9c)$$

$$\gamma_n = \frac{k_x\beta_n^2}{C} \quad (9d)$$

where β_n is the root of the transcendental equation: $\beta_n e_b \cot an(\beta_n e_b) + (2k_{ev}A_{ev}e_b/\lambda_{ev}k_xS_b) = 0$.

-Case 2:

In this case, due to the symmetry of the system layout, only one half of the domain is studied. The boundary conditions are then given as:

$$\begin{aligned} &T(x,0) - T_{in} = 0 \\ &\tfrac{\partial(T-T_{in})}{\partial x}(x = 0, t) = 0 \\ &\left(\tfrac{\partial(T-T_{in})}{\partial x} + F(T - T_{in})\right)(x = e_c, t) = f(t) \\ &f(t = 0) = 0 \\ &e_c = \tfrac{e_b}{2} \end{aligned} \quad (10)$$

The solution can thus be acquired as:

$$T_i(x,t) - T_{in} = \sum_{n=0}^{\infty}(H_0(t) - H_0(0)\exp(-\mu_n t))\cos(\alpha_n x) - \cos\left(\frac{\pi x}{e_c}\right)\frac{f(t)}{F} \quad (11a)$$

$$\Omega_n H_0(t) = \frac{\cos(\alpha_n e_c)}{\left(\frac{\pi}{e_c}\right)^2 - \alpha_n^2}f(t) + \frac{Ri^2\sin(\alpha_n e_c)}{k_x\alpha_n^3} + \left(\frac{k_x\cos(\alpha_n e_c)}{C}\right) \times \left[\int_0^t f(t)\exp(\mu_n t)dt\right]\exp(-\mu_n t) \quad (11b)$$

$$\Omega_n = \frac{\alpha_n e_c + \cos(\alpha_n e_c)\sin(\alpha_n e_c)}{2\alpha_n} \quad (11c)$$

$$\mu_n = \frac{k_x\alpha_n^2}{C} \quad (11d)$$

where α_n is the root of the transcendental equation: $\alpha_n e_c \tan(\alpha_n e_c) = Fe_c$.

Both solutions (for Cases 1 and 2 with heat pipes) can be conveniently modified for convective cooling. For replacing the heat pipes by convective cooling, the minor modifications are:

$$f(t) = 0; \quad \frac{k_{ev}A_{ev}}{\lambda_{ev}} = hS_b \quad (12)$$

The analytical model will be used as the reference in certain cases and compared to the 1D computational model and the 3D numerical simulation. Unlike the 1D analytical model, the 1D computational model, as presented in the following sub-section, is able to simulate the battery cell cooling by the heat pipe set in different configurations without using vapour temperature function or experimental data.

4.2. One-dimensional computational model

Fig. 8 presents the 1D computational model of the battery in conjunction with the heat pipe set, based on the thermal circuit method where the battery is represented by a thermal network. A number of nodes are chosen in the battery and linked by a thermal resistance (or thermal conductance) depending upon the thermo-physical and geometrical properties of the battery. The transient behaviour of the model is obtained by allocating a thermal capacitance to each node, as seen in Fig. 8(b). Each node occupies a volume and generates a thermal power proportional to its volume.

The preliminary analyses suggest that five nodes are enough to represent the thermal behaviour of the battery considered. The 1D

computational approach offers a possibility to treat the battery and heat pipe models separately. Based on this, more nodes can be easily added for a larger battery, without modifying the heat pipe model and the calculation process. It should be noted that the number of nodes for modelling the battery can be optimised using the 1D analytical model derived before. R_{bij} is the thermal resistance between the nodes i and j in the battery cell. The complete model of the battery (using five nodes) connected to the heat pipe set thermal model (four nodes) is represented by the nodal temperature matrix:

$$[C]\frac{d[T]}{dt} = [G][T] + [P] \quad (13)$$

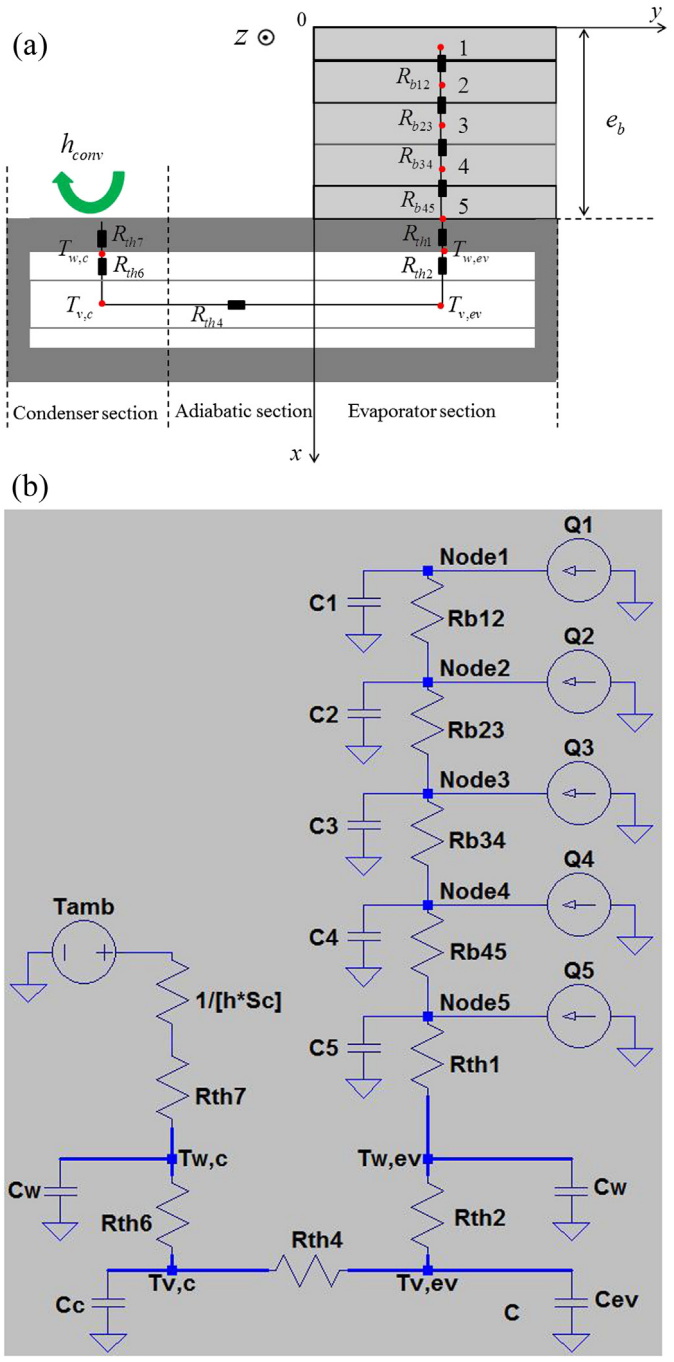

Fig. 8. Nodes of the 1D computational model of the battery connected to the heat pipe set. (a) Steady state model. (b) transient model.

This equation can also be used for convective cooling by just removing the nodes of the heat pipe and adding the term due to the convective coefficient.

4.3. Three-dimensional numerical simulation

The global thermo-physical properties derived in Eq. (4) are used in the 3D numerical model. The cooling solution is applied on the battery surface in the x direction ($x = 0$ and $x = e_b$). Therefore the other battery surfaces in y and z directions develop a free natural convection. For modelling this natural convection, a heat coefficient $h_{conv} = 5\ W\ m^{-2}\ K^{-1}$ is chosen as an example in this study.

Different scenarios are investigated, from constant temperature to forced convection. However, the complexity of the heat pipe does not allow a transient simulation of the battery cooled by the heat pipe set at the moment. Nevertheless, an equivalent conductance per surface area of the heat pipe set can be calculated and used as an input in the CFD code. More details on this approach will be presented in Sub-section 5.4. The mesh of the 3D battery model is refined in the x direction, as shown in Fig. 9, in order to observe properly the expected large temperature gradient and to compare the results with the 1D analytical and computational approaches.

5. Results and discussions

In this section, the 1D computational model developed is analysed in various configurations and compared to the 1D analytical model and the 3D numerical simulation, so as to demonstrate the advantages of the 1D approach in view of the reliability and effectiveness. The results presented will verify if the heat pipe set designed and the distributed configuration recommended are able to meet the requirements of the temperature specifications [10].

5.1. Forced convection and fixed temperature

In this configuration, the battery surface located at $x = 0$ has a fixed temperature ($T(0,t) = T_{amb} = 20\ °C$) and a convective heat coefficient ($h = 20\ W\ m^{-2}\ K^{-1}$) on the surface located at $x = e_b$. Moreover, for the 3D numerical simulation, natural convection ($h = 5\ W\ m^{-2}\ K^{-1}$) is considered on the surfaces in y and z directions. Fig. 10 presents the results obtained from the 3D numerical simulation at the end of the transient simulation. The results show that the gradient of temperature is mainly located in the x direction. Moreover the temperature in the YZ plane can be considered as uniform. In fact at $x = e_b$, the temperature difference between the maximum and minimum temperatures in the YZ plane is $\Delta T(x = e_b) = 0.042\ °C$.

The temperature at the different battery locations is compared for the three cases, i.e. 3D simulation and 1D analytical and computational cases. Table 2 classifies the different points studied and their equivalents in the different models, in order to simplify the presentation of the results in Fig. 11. The comparison of the temperature rises for the three cases is presented in Fig. 11. The results clearly show that for the different locations considered in the battery (Table 2), all the three cases (3D and 1D) yield very similar temperature predictions in both the transient and steady states. Moreover, the results suggest that there is a small discrepancy between the 1D computational and analytical models, as seen in Fig. 11. Table 3 further summarises the temperature difference between the 1D computational and analytical models in a quantitative format, which indicates the very small discrepancy (less than 0.5%) at the end of the simulation, predicted by these two models.

The discrepancy of temperature between the 1D computational model and 3D numerical model at the end of the simulation is 0.01%. Therefore, the 1D computational model is sufficient to

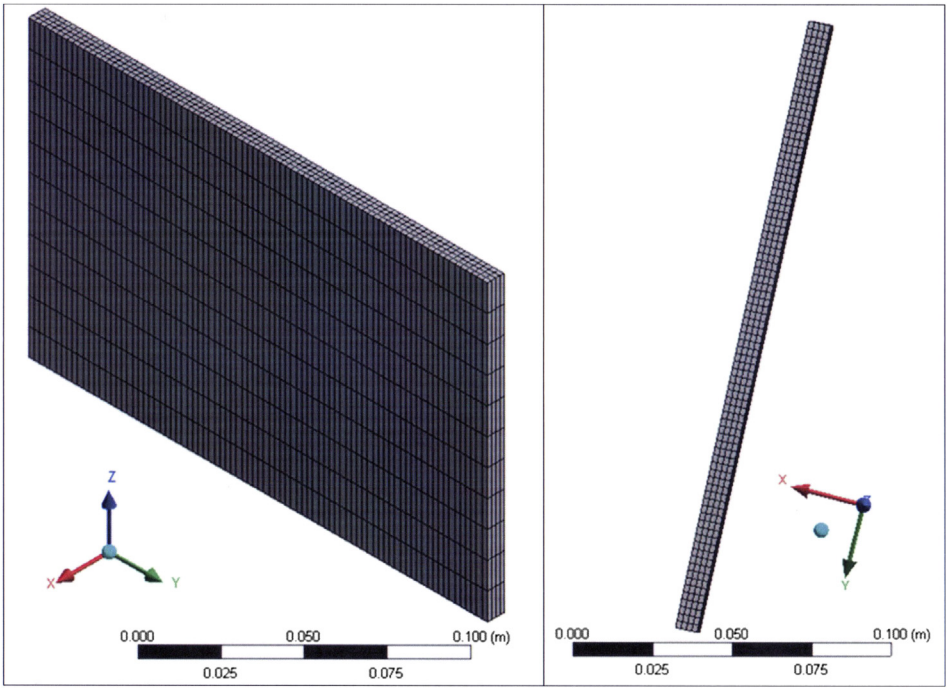

Fig. 9. Mesh of the battery cell in the 3D numerical simulation.

describe the transient behaviour of the battery cell. This result was predictable using the Biot Number (*Bi*). This number compared the thermal resistance of conduction with the thermal resistance of convection. Therefore the condition, $Bi << 1$, indicates that the temperature in a body can be considered uniform [9]: $Bi_j = h_j L_j / k_j$ with j indicating the direction *x*, *y*, *z*.

Table 4 shows that the Biot numbers in the *y* and *z* directions are much less than one. As a consequence, the temperature in the YZ plan can be considered uniform. Additionally, the 3D numerical model used 18,895 nodes, where the 1D computational model used only 5 nodes. The running time of the 1D computational model took much shorter time than the 3D numerical simulation. The run time needed for the 1D computational model is comparable to the analytical solution, which takes almost no time to run.

5.2. Theoretical test of linear temperature vapour in the heat pipe

This sub-section attempts to verify the analytical model (Eqs. (9a)–(9c)) in Case 1 with $f(t) \neq 0$. In this case, one surface has a fixed temperature, and the other is cooled by a heat pipe set. The formulation $f(t) = F(T_v(t) - T_{in})$ is calculated with a prescribed vapour temperature. The characteristics of the vapour temperature could vary, which could be represented by a linear or nonlinear function. To simply the analysis, a linear function is chosen to perform the calculations. For a relative comparison, the analytical formulation of the vapour temperature can be used which is given by $T_v(t) = 10t/550 + 20$, where the slope 10/550 is chosen to represent a mild temperature variation. Based on these assumptions, the 1D computational model and analytical solution are compared, and the results are presented in Fig. 12.

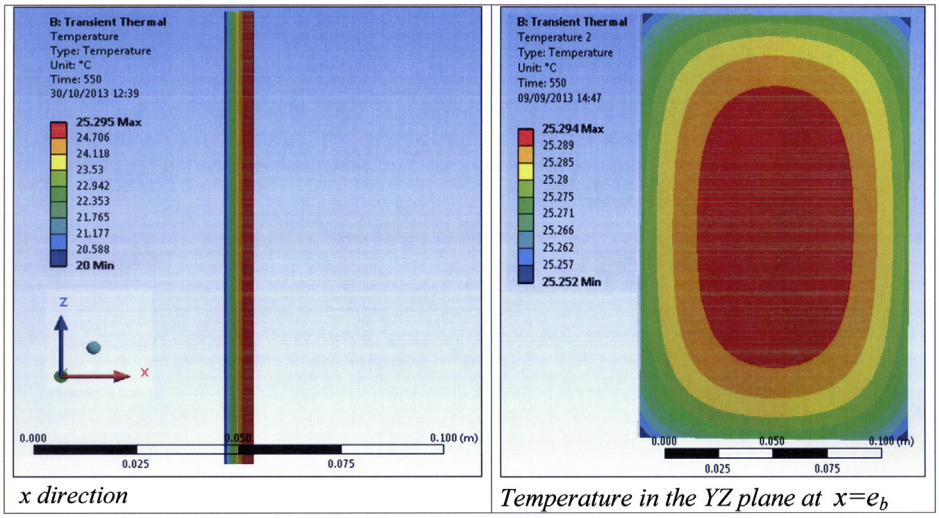

Fig. 10. Temperature distribution of the battery with fixed temperature and convective heat transfer coefficient.

Table 2
Position of the nodes studied for the 1D analytical and numerical models.

1D computational	1D analytical	Position of the node (m)
T1	$x = eb/16$	0.0004375
T2	$x = 2^*(eb/8)$	0.00175
T3	$x = 4^*(eb/8)$	0.0035
T4	$x = 6^*(eb/8)$	0.00525
T5	$x = 8^*(eb/8)$	0.007

Table 3
Discrepancy of temperature between the 1D computational and analytical models.

Position of the node (m)	1D computational	1D analytical	Discrepancy
4.38E-04	20.709	20.686	0.11%
1.75E-03	22.553	22.461	0.41%
3.50E-03	24.253	24.164	0.37%
5.25E-03	25.195	25.109	0.34%
7.00E-03	25.380	25.297	0.33%

The results show a good agreement between the numerical and the analytical solutions, which confirms the effectiveness of the derived analytical solution for a boundary condition that is dependent upon the time. Thus, the analytical model proposed in this study can be used for practical applications with different types of cooling methods.

5.3. Battery cell sandwiched by two heat pipe sets

The battery sandwiched by two heat pipe sets is presented in Fig. 13, which might be the case in view of large battery packs for electric vehicles. The other cooling solution, forced convection (CS1) directly applied on the battery's surfaces, is compared with the heat pipe cooling solution (CS2, shown in Fig. 14). For a proper comparison, identical convective coefficients ($h = 28\ \mathrm{W\ m^{-2}\ K^{-1}}$) are used for the condensing area of the heat pipe set and also for the convective cooling within the both cooling solutions, respectively. Fig. 15 presents the comparison of the characteristics of the maximum temperature in a battery cell for the CS1 and CS2 cooling solutions.

The efficiency of the heat pipe set depends on its design parameters but also on the cooling process used at the condenser. Contrary to CS1, the heat pipe set (CS2) yields a larger contact area for the same convective heat transfer coefficient. For the simulation conditions considered in this study, the contact areas of CS1 and CS2 can be calculated as: $S_b = 0.0244\ \mathrm{m^2}$ and $S_c = 0.14\ \mathrm{m^2}$, respectively. The gap between the heat pipes in the set is 0.8 mm. These gaps allow the cooling fluid to flow around the pipes, which improves the cooling efficiency of the system. It should be noted that the type and design of the cooling process at the condenser have an effect on the S_c value of the heat pipe set. In order to simplify the analysis and to be conservative as well, the minimum contact area at the condenser, $S_c = 0.14\ \mathrm{m^2}$, is considered.

The maximum temperature is obtained for both cooling solutions, namely 51.5 °C for CS1 and 27.6 °C for CS2. For the convective heat transfer coefficients considered, using heat pipes yields better cooling than the forced convection. Furthermore, an even temperature distribution in the battery cell must be achieved in order to avoid safety issues. Half of the battery is represented in Fig. 15, because of the symmetric cooling configuration. The temperature difference between the maximum and the minimum is less than 2 °C for both cooling solutions. The steady state is reached faster using the heat pipe set. In fact, the approximations or models used (conductance calculation) were chosen to achieve better performances for a real application. Moreover, the efficiency of the heat pipe set in distributed configuration can be significantly improved by:

- An efficient cooling of the condenser.
- Increasing the length of the condenser.
- Adding fins to the heat pipe sets.

The complexity of the heat pipe does not allow a simple CFD simulation. Additionally, the analytical model developed needs an expression or experimental data of the vapour temperature. The approach developed using an equivalent conductance of the heat pipe proves to be effective, in which the 1D computational model of the battery is connected to the heat pipe. It is therefore taken as the reference to study the impact of the equivalent conductance.

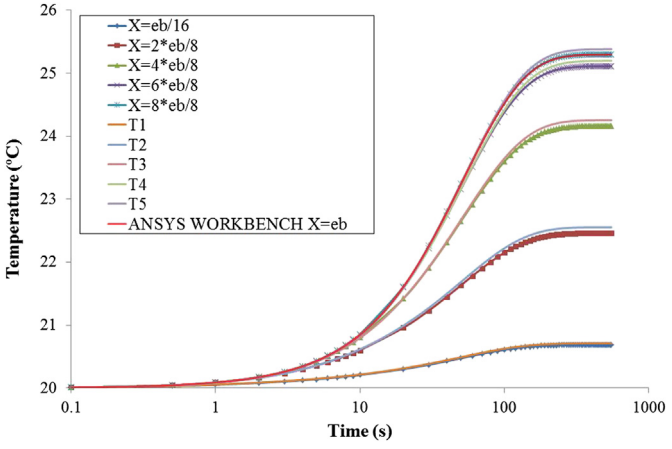

Fig. 11. Battery cell temperature with fixed temperature and convective heat transfer coefficient for the three cases.

5.4. Equivalent thermal conductance of the heat pipe

To achieve a further simplified formulation, the equivalent thermal conductance is defined and calculated using the thermal network of the heat pipes. The analogy between the thermal network (Fig. 6) and the electric circuit is used to derive the equivalent thermal conductance:

$$G_{eq} = \left(R_{th1} + R_{th2} + R_{th6} + R_{th7} + \frac{1}{hS_c}\right)^{-1} = 3.37\ \mathrm{W\ K^{-1}} \quad (14)$$

The equivalent convective heat coefficient can correspondingly be defined and obtained by:

$$h_{eq} = G_{eq}/S_b \quad (15)$$

Based on the above definition of equivalent convective heat coefficient, Figs. 16 and 17 depict the performance characteristics of the maximum and minimum temperatures of the battery cell for heat pipes. The results suggest that using the equivalent model defined in Eqs. (14) and (15) yields good approximation of both maximum and minimum temperature to those generated by the complete thermal network model of the heat pipes. However, the

Table 4
Directional Biot number.

Direction	k	h	L	Bi
x	0.97	20.00	0.007	0.14
y	26.57	5.00	0.195	0.04
z	26.57	5.00	0.125	0.02

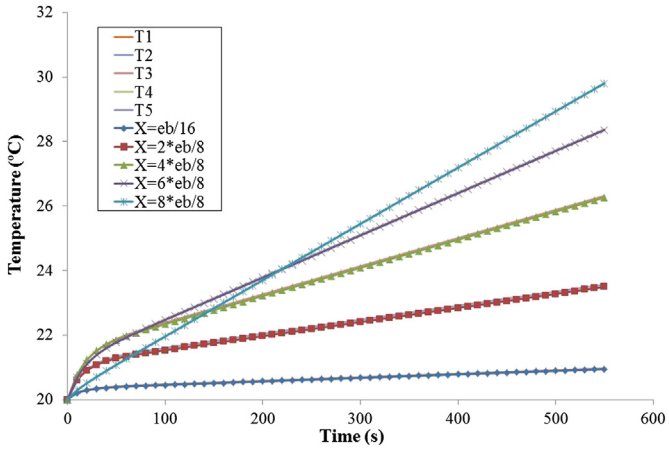

Fig. 12. Comparison of battery temperature between the 1D computational and analytical models with a linear vapour temperature in the heat pipe.

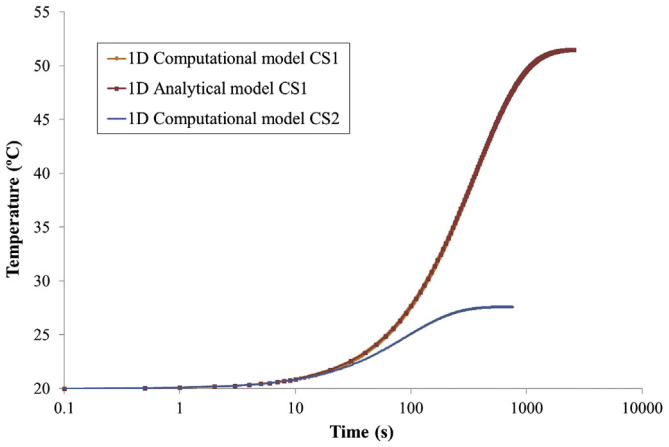

Fig. 14. Comparison of maximum temperature for the forced convection (CS1) and heat pipe set (CS2) in a distributed configuration using the same convective heat coefficient.

computational efficiency based on the equivalent model is improved in the CFD simulation. It should be noted that the CFD simulation of the transient thermal dynamics of the battery with heat pipes is computationally very demanding. Therefore, the proposed equivalent model offers a feasible solution for conducting design and analysis of battery cooling systems at the preliminary design stage.

It is also observed from the results that the equivalent approach tends to overestimate the temperature rise, which might be attributed to the conservatism in the parameter determination including the intensity of the convection in the condensing area and the model simplifications. The discrepancy observed between the approaches is due to the thermal capacity of the heat pipe. In the complete 1D computational model, the thermal capacity evolves with the temperature during the simulation process, but the equivalent conductance approach does not consider the thermal capacity and therefore reaches the steady state faster, as seen in Figs. 16 and 17.

5.5. Thermodynamic process within the heat pipe

The heat pipe is oversized using the working fluid merit number method, which helps to achieve the heat pipe design in a more practical way. Zuo and Faghri [19] proposed a method based on the first law of thermodynamics. The liquid sub-cooling is a requirement for the heat pipe operation when the liquid is travelling from the condenser to the evaporator [19]. This sub-cooling requirement can thus be met if [19]:

$$\Psi = \Phi/\Theta > 1 \tag{16}$$

where $\Phi = (b/2R_{HP})(R_v^4/L_c(L_e + 2L_a + L_c))$; $\Theta = 2k_{ev}(T_{HP}\mu_v/(\rho_v h_{fg})^2)$; and $T_{HP} = (T_{v,\,ev} + T_{v,\,c}/2)$.

In the above equation, Φ represents the geometric group (a group of geometrical parameters of the heat pipes), and Θ represents the thermo-physical group (a group of thermo-physical properties of the working fluid).

Fig. 18 presents the variation of the minimum value of Ψ, calculated from Eq. (16), over the vapour temperature range considered, using the 1D computational model. It can be clearly seen that the Ψ value is the order of 10^6 and much larger than 1, which satisfies the sub-cooling requirement. The very large value of Ψ is primarily due to the oversizing in the heat transfer capacity of the heat pipe.

6. Concluding remarks

An analysis of the passive cooling management of the ePLB C020 battery cell by heat pipes was studied in this paper. A one-dimensional approach composed of a 1D computational model of the battery connected to a thermal network of the heat pipe, is

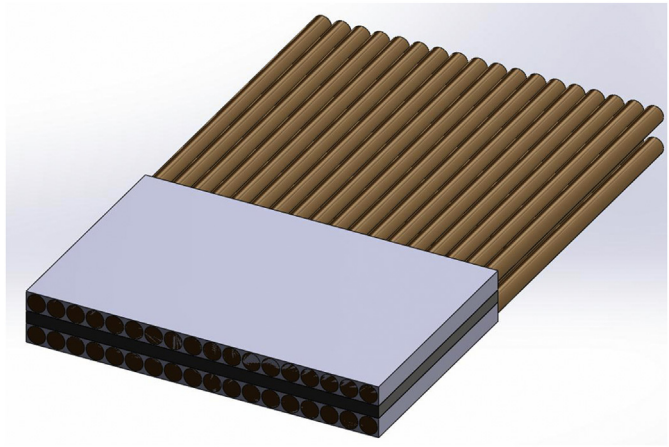

Fig. 13. Battery cell sandwiched by two heat pipe sets.

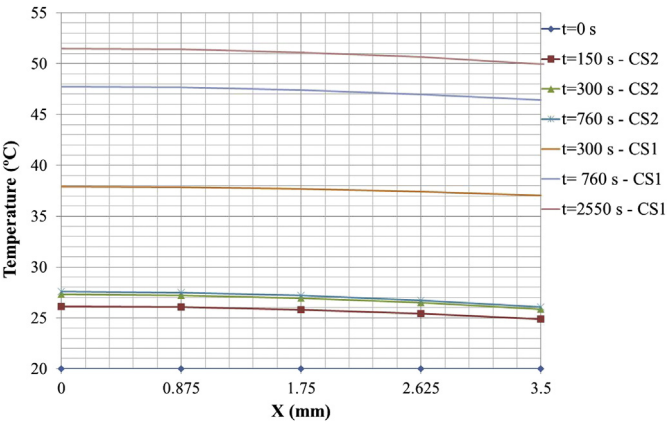

Fig. 15. Comparison of temperature distribution between CS1 and CS2.

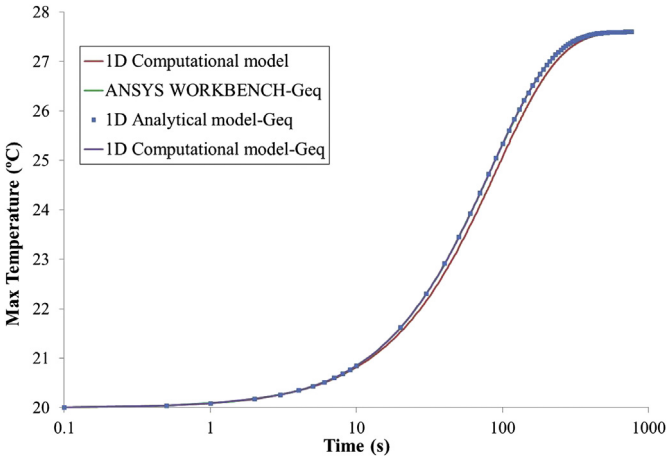

Fig. 16. Maximum temperature of the battery cell using different approaches for the heat pipe set.

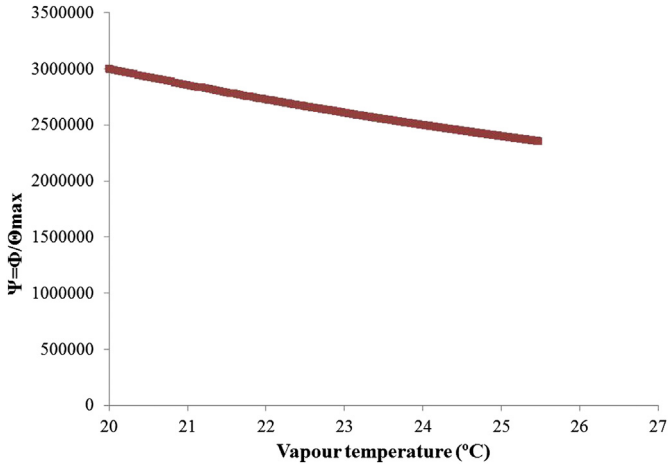

Fig. 18. Verification of the sub-cooling condition of the heat pipe operation, using the method proposed in Ref. [19].

proposed. This approach is based on the thermal circuit method and allows to treat the battery and the heat pipe separately. An analytical model with time-dependent boundary conditions and a 3D numerical model were developed in order to test and verify certain hypotheses made for the one-dimensional computational approach.

The lack of experimental data for this study made it difficult to systematically assess the design and modelling approaches. Accordingly the design of the cooling system was made intentionally conservative. Because of this, the heat generation of the battery was taken as a constant at the maximum rate of discharge. Simplifications were also made concerning the model of the heat pipe and its design. Regarding the thermal network model of the heat pipe, the thermal resistance at the evaporator was calculated using the Chi model. The Chi model is very conservative and was useful for this study but not recommended when the size of the heat pipe is a critical issue. Besides, the impact of the liquid film at the condenser was approximated by an experimental factor [17]. Moreover, the design of the heat pipe did not take into account the reduction of the liquid section at the evaporator and the impact of the gravity. In addition, the effect between each heat pipe was neglected in the heat pipe set.

The comparison between the 1D model (computational and analytical) and the 3D numerical simulation by CFD showed a good agreement. The results confirmed the reliability of the one-dimensional approach to simulate the thermal behaviour of the battery cell. Besides, the 1D approach takes much shorter running time than the 3D numerical simulation. Because of this, the 1D approach holds great potentials for practical applications. However, the results cannot be generalized since they depend on the Biot number of the system.

The heat pipe set designed and applied on the battery cell in a distributed configuration was studied using the 1D computational model. This simulation made with conservative correlations and approximations for the heat pipe model, predicted a maximum temperature of 27.6 °C. A maximum temperature of 51.5 °C is obtained for the same configuration in a forced convection cooling directly applied on the surface of the battery. The results with a conservative design and calculation showed the importance of the heat pipe and the effectiveness of the passive cooling management.

The thermal network model of the heat pipe will be further studied experimentally in order to verify the impact of the approximations and hypotheses made in following-on researches. Experimental data of the battery cell will allow the addition of a heat generation term depending on time in the cooling system model (numerical and analytical). Therefore, a future study will target the thermal behaviour of the battery during practical driving scenarios. The final goal will be to extend this study to a battery pack with the heat pipe sets in a distributed configuration (each cell sandwiched by two heat pipe). Supplementary to this study, nanotube of copper can also be investigated in order to improve the thermo-physical properties of the heat pipe material.

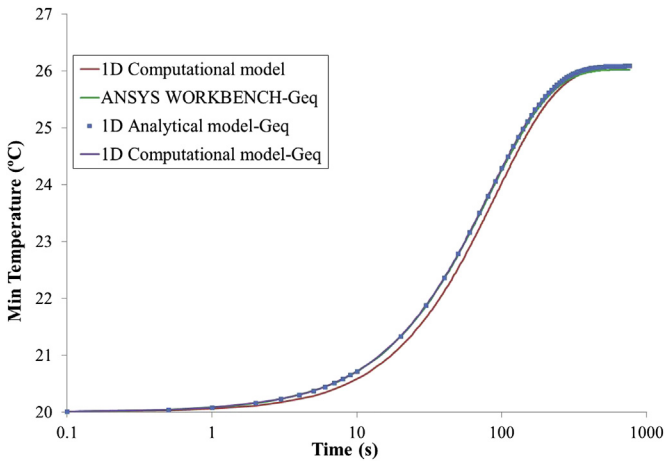

Fig. 17. Minimum temperature of the battery cell using different approaches for the heat pipe set.

References

[1] L. Lu, X. Han, J. Li, J. Hua, M. Ouyang, J. Power Sources 226 (2013) 272–288.
[2] Z. Rao, S. Wang, Renew. Sustain. Energy Rev. 15 (2011) 4554–4571.
[3] L. Gao, S. Liu, A. Dougal, IEEE Trans. Compon. Packag. Technol. 25 (2002) 495–505.
[4] S.X. Chen, K.J. Tseng, S.S. Choi, IEEE Power Energy Soc. (2009) 1–4.
[5] Y. Inui, Y. Kobayashi, Y. Watanabe, Y. Watase, Y. Kitamura, Energy Convers. Manag. 48 (2007) 2103–2109.
[6] G. Karimi, X. Li, Int. J. Energy Res. 37 (2013) 13–24.
[7] C. Lin, K. Chen, F. Sun, P. Tang, H. Zhao, in: Vehicle Power and Propulsion Conference, VPPC'09, IEEE, 2009, pp. 1643–1648.
[8] M.C. Niculuta, C. Veje, J. Phys. Conf. Ser. 395 (2012) 012013.
[9] P. Taheri, M. Bahrami, SAE Int. J. Passenger Cars Electron. Electr. Syst. 5 (1) (2012) 164–176.
[10] A.A. Pesaran, J. Power Sources 110 (2002) 377–382.
[11] S. Chacko, Numerical Analysis of Unsteady Heat Transfer for Thermal Management (Ph. D.), Warwick University, United Kingdom, 2012.
[12] R. Mahamud, C. Park, J. Power Sources 196 (2011) 5685–5696.

[13] Z.H. Rao, S.F. Wang, Y.L. Zhang, J. Energy Inst. 85 (1) (2012) 38–43.
[14] M.Y. Ramandi, I. Dincer, G.F. Naterer, Heat Mass Transf. 47 (2011) 777–788.
[15] M.S. Wu, K.H. Liu, Y.Y. Wang, C.C. Wan, J. Power Sources 109 (2002) 160–166.
[16] Z. Rao, S. Wang, M. Wu, Z. Lin, F. Lin, Energy Convers. Manag. 65 (2013) 92–97.
[17] C. Romestant, Etudes théoriques et expérimentales de caloducs et de thermosiphons soumis à de fortes accélérations (Ph. D.), ENSMA (Ecole Nationale Supérieur de Mécanique et d'Aérotechnique), France, 1992.
[18] R. Bertossi, Modélisation des transferts de chaleur et de masse dans les caloducs: Contribution à l'analyse des phénomènes d'interfaces intervenant dans écoulements diphasiques (Ph. D.), ENSMA (Ecole Nationale Supérieur de Mécanique et d'Aérotechnique), France, 2009.
[19] Z.J. Zuo, A. Faghri, Int. J. Heat Mass Transf. 41 (11) (1998) 1473–1484.
[20] Y. Avenas, Etude et réalisation de caloducs plats miniatures pour l'intégration en électronique de puissance (Ph. D.), INPG (Institut National Polytechnique de Grenoble), France, 2009.
[21] S. Saedodin, M. Torabi, Adv. Theor. Appl. Mech. 3 (2010) 369–383.